

# Efficiency of evanescent excitation and collection of spontaneous Raman scattering near high index contrast channel waveguides

Ashim Dhakal,\* Ali Raza, Frédéric Peyskens, Ananth Z. Subramanian, Stéphane Clemmen, Nicolas Le Thomas and Roel Baets

Photonics Research Group, INTEC Department-Gent University-imec, Center for Nano- and Biophotonics, Ghent University, 9000 Gent, Belgium

\*ashim.dhakal@intec.ugent.be

**Abstract:** We develop and experimentally verify a theoretical model for the total efficiency  $\eta_0$  of evanescent excitation and subsequent collection of spontaneous Raman signals by the fundamental quasi-TE and quasi-TM modes of a generic photonic channel waveguide. Single-mode silicon nitride ( $\text{Si}_3\text{N}_4$ ) slot and strip waveguides of different dimensions are used in the experimental study. Our theoretical model is validated by the correspondence between the experimental and theoretical absolute values within the experimental errors. We extend our theoretical model to silicon-on-insulator (SOI) and titanium dioxide ( $\text{TiO}_2$ ) channel waveguides and study  $\eta_0$  as a function of index contrast, polarization of the mode and the geometry of the waveguides. We report nearly 2.5 (4 and 5) times larger  $\eta_0$  for the fundamental quasi-TM mode when compared to  $\eta_0$  for the fundamental quasi-TE mode of a typical  $\text{Si}_3\text{N}_4$  ( $\text{TiO}_2$  and SOI) strip waveguide.  $\eta_0$  for the fundamental quasi-TE mode of a typical  $\text{Si}_3\text{N}_4$  ( $\text{TiO}_2$  and SOI) slot waveguide is about 7 (22 and 90) times larger when compared to  $\eta_0$  for the fundamental quasi-TE mode of a strip waveguide of the similar dimensions. We attribute the observed enhancement to the higher electric field discontinuity present in high index contrast waveguides.

©2015 Optical Society of America

**OCIS codes:** (130.0130) Integrated optics; (170.5660) Raman spectroscopy; (130.6010) Sensors; (230.6080) Sources.

---

## References and Links

1. X. Fan, I. M. White, S. I. Shopova, H. Zhu, J. D. Suter, and Y. Sun, "Sensitive optical biosensors for unlabeled targets: A review," *Anal. Chim. Acta* **620**(1-2), 8–26 (2008).
2. E. Ryckeboer, R. Bockstaele, M. Vanslembrouck, and R. Baets, "Glucose sensing by waveguide-based absorption spectroscopy on a silicon chip," *Biomed. Opt. Express* **5**(5), 1636–1648 (2014).
3. A. Dhakal, A. Z. Subramanian, P. Wuytens, F. Peyskens, N. L. Thomas, and R. Baets, "Evanescent excitation and collection of spontaneous Raman spectra using silicon nitride nanophotonic waveguides," *Opt. Lett.* **39**(13), 4025–4028 (2014).
4. D. A. Long, *The Raman Effect: A Unified Treatment of the Theory of Raman Scattering by Molecules* (John Wiley & Sons, Ltd, 2002).
5. A. Dhakal, P. Wuytens, F. Peyskens, A. Z. Subramanian, N. Le Thomas, and R. Baets, "Nanophotonic lab-on-a-chip Raman sensors: a sensitivity comparison with confocal Raman microscope," in *IEEE BioPhotonics Conference* (IEEE, 2015).
6. N. Ismail, L.-P. Choo-Smith, K. Wörhoff, A. Driessen, A. C. Baclig, P. J. Caspers, G. J. Puppels, R. M. de Ridder, and M. Pollnau, "Raman spectroscopy with an integrated arrayed-waveguide grating," *Opt. Lett.* **36**(23), 4629–4631 (2011).
7. Y. C. Jun, R. M. Briggs, H. A. Atwater, and M. L. Brongersma, "Broadband enhancement of light emission in silicon slot waveguides," *Opt. Express* **17**(9), 7479–7490 (2009).
8. L. Novotny, "Allowed and forbidden light in near-field optics. I. A single dipolar light source," *J. Opt. Soc. Am. A* **14**(1), 91–104 (1997).

9. A. Dhakal, A. Z. Subramanian, N. L. Thomas, and R. Baets, "The role of index contrast in the efficiency of absorption and emission of a luminescent particle near a slab waveguide," in *16th European Conference on Integrated Optics* (ECIO, 2012), 131.
10. A. Dhakal, A. F. Peyskens, A. Subramanian, N. Le Thomas, and R. Baets, "Enhancement of light absorption, scattering and emission in high index contrast waveguides," in *Advanced Photonics 2013*, OSA Technical Digest (online) (OSA, 2013), paper ST2B.5.
11. A. Dhakal, F. Peyskens, A. Z. Subramanian, N. Le Thomas, and R. Baets, "Enhanced spontaneous Raman signal collected evanescently by silicon nitride slot waveguides" in *CLEO: 2015*, OSA Technical Digest (online) (OSA, 2015), paper STh4H.3.
12. A. Z. Subramanian, P. Neutens, A. Dhakal, R. Jansen, T. Claes, X. Rottenberg, F. Peyskens, S. Selvaraja, P. Helin, B. Du Bois, K. Leysens, S. Severi, P. Deshpande, R. Baets, and P. Van Dorpe, "Low-loss singlemode PECVD silicon nitride photonic wire waveguides for 532–900 nm wavelength window fabricated within a CMOS pilot line," *IEEE Photonics J.* **5**(6), 2202809 (2013).
13. C. A. Barrios, B. Sánchez, K. B. Gylfason, A. Griol, H. Sohlström, M. Holgado, and R. Casquel, "Demonstration of slot-waveguide structures on silicon nitride / silicon oxide platform," *Opt. Express* **15**(11), 6846–6856 (2007).
14. W. Bogaerts, R. Baets, P. Dumon, V. Wiaux, S. Beckx, D. Taillaert, B. Luyssaert, J. Van Campenhout, P. Bienstman, and D. Van Thourhout, "Nanophotonic waveguides in silicon-on-insulator fabricated with CMOS technology," *J. Lightwave Technol.* **23**(1), 401–412 (2005).
15. M. Häyriäinen, M. Roussey, A. Säynätjoki, M. Kuittinen, and S. Honkanen, "Titanium dioxide slot waveguides for visible wavelengths," *Appl. Opt.* **54**(10), 2653–2657 (2015).
16. C. C. Evans, C. Liu, and J. Suntivich, "Low-loss titanium dioxide waveguides for integrated evanescent raman spectroscopy," in *CLEO: 2015*, OSA Technical Digest (online) (OSA, 2015), paper SM3O.4.
17. V. Mazet, C. Carteret, D. Brie, J. Idier, and B. Humbert, "Background removal from spectra by designing and minimising a non-quadratic cost function," *Chemom. Intell. Lab. Syst.* **76**(2), 121–133 (2005).
18. M. J. Colles and J. E. Griffiths, "Relative and absolute Raman scattering cross sections in liquids," *J. Chem. Phys.* **7**(56), 3384 (2003).
19. N. R. Draper and H. Smith, *Applied Regression Analysis* (Wiley-Interscience, 1998).
20. S. Bisschop, A. Guille, D. Van Thourhout, Z. Hens, and E. Brainis, "Broadband enhancement of single photon emission and polarization dependent coupling in silicon nitride waveguides," *Opt. Express* **23**(11), 13713–13724 (2015).
21. T. J. Kippenberg, J. Kalkman, A. Polman, and K. J. Vahala, "Demonstration of an erbium-doped microdisk laser on a silicon chip," *Phys. Rev. A* **74**(5), 051802 (2006).
22. D. Liang, G. Roelkens, R. Baets, and J. E. Bowers, "Hybrid integrated platforms for silicon photonics," *Materials (Basel)* **3**(3), 1782–1802 (2010).
23. A. W. Snyder and J. D. Love, *Optical Waveguide Theory* (Chapman and Hall New York, 1983).
24. W. Herr, B. J. Holzer, and B. Muratori, "Chapter 6.4 Concept of luminosity," in *Accelerators and Colliders* (Springer Berlin, 2013), pp. 140–146.

## 1. Introduction

Integrated photonics has been established as a very promising platform for lab-on-a-chip sensing applications [1]. An emergent type of photonic sensors is based on light-matter interaction with the evanescent wave of nanophotonic waveguide modes. This has led to the realization of on-chip absorption spectroscopy [2] and spontaneous Raman spectroscopy [3]. These spectroscopic sensors, particularly Raman sensors, allow for direct detection and analysis of the target molecules by measuring their distinctive spectrum [4]. In this paper we consider Raman sensors in which the molecules under study are evanescently excited through a high-index channel waveguide and the corresponding Raman signal is evanescently collected using the same single-mode photonic waveguide. This technique leads to a signal much stronger than collected by Raman microscopes, thanks to a long interaction length and the enhancement effects inherent to high-index-contrast waveguides [5]. In the proposed technique, a single-mode waveguide carries the pump beam and also collects the Stokes light with the smallest possible étendue. Hence, it opens up the potential of integration with very compact photonic components, such as an Arrayed Waveguide Grating (AWGs) acting as an on-chip spectrometer [6]. Furthermore, these nanophotonic chips are mass-producible at the wafer scale using CMOS-compatible process steps, which will pave the way towards low-cost, high performance and compact point-of-need tools for Raman analysis of chemical and biological materials.

To achieve the best performance of these sensors, it is crucial to optimize the various design parameters of the waveguide, such as geometry, dimensions, polarization of the mode

and the index contrast. The corresponding problem can be modelled as a scattering problem or as an absorption/re-emission problem near a waveguide. The absorption and emission of light by the particles lying close to planar dielectric waveguides is studied extensively in the context of light sources and sensors [7–10]. In this paper we complement these studies in the context of channel waveguides that are used extensively in integrated photonics. We will study the overall conversion efficiency ( $\eta_0$ ) which is defined as the ratio between the total Stokes power ( $P_{wg}$ ) collected (in both directions) by a waveguide of unit length to the pump power ( $P_{in}$ ) in the same waveguide for unit scattering cross section when the particles are distributed uniformly in the vicinity of the waveguide with unit concentration [3]. We will elaborate the preliminary theoretical analysis and experimental results reported earlier [3, 10, 11]. In particular, we will experimentally validate the key equation for  $\eta_0$  in an absolute manner and investigate how  $\eta_0$  is affected by the polarization of the mode, the refractive index contrast, and the waveguide geometry.

In section 2, we outline the experimental methodology and compare the experimental results with the theoretical values of  $\eta_0$  obtained for both quasi-TE (henceforth, *TE*) and TM (henceforth, *TM*) polarizations for silicon nitride ( $\text{Si}_3\text{N}_4$ ) strip [12] and slot [13] waveguides of several widths. In section 3 we discuss the experimental results with the help of more detailed simulation results. In section 3 we also extend the theoretical analysis to silicon-on-insulator (SOI) waveguide platform [14] and an emerging waveguide platform based on Titanium oxide ( $\text{TiO}_2$ ) [15, 16] to assess their performance as evanescent sensors or light sources. The derivation of the key equation for determining  $\eta_0$  is elaborated in the Appendix.

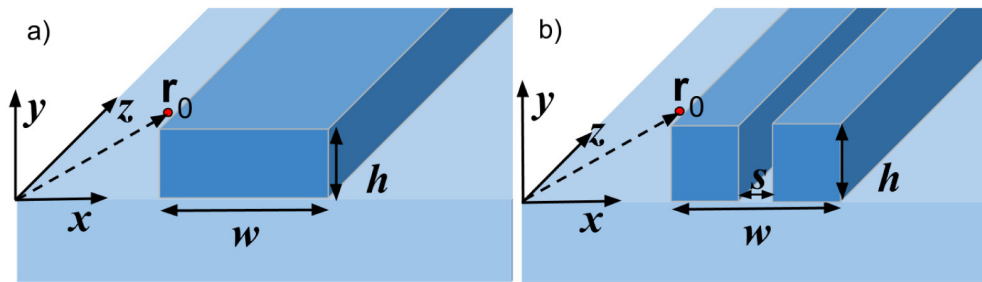


Fig. 1. Schematic of a dielectric a) strip and b) slot waveguides defined by a core of higher refractive index ( $\text{Si}_3\text{N}_4$ ,  $\text{TiO}_2$  or silicon) patterned on a lower index bottom cladding (typically silicon dioxide). The scattering particles are assumed to be embedded with a uniform density in the upper cladding (colorless region). A particle at position  $\mathbf{r}_0$  is shown for both cases for theoretical analysis in the Appendix.

## 2. Measurement of $\eta_0$ for strip and slot $\text{Si}_3\text{N}_4$ waveguides

We consider a nanophotonic waveguide that is translationally invariant along its length  $L$  ( $z$ -axis in Fig. 1) and assume that the scattering particles with cross-section  $\sigma$  lie uniformly in the upper cladding with a density  $\rho$ . As discussed in [3], to measure the conversion efficiency  $\eta_0$  for several waveguides it is convenient to define the guided power efficiency  $\zeta(L)$  as the ratio of the spontaneous Stokes power collected by the waveguides  $P_{col}$  to the transmitted pump power  $P_{tx}$ . The quantity  $\eta_0$  is related directly to  $\zeta(L)$  via:

$$\zeta(L) \equiv \frac{P_{col}(L)}{P_{tx}} = \frac{1}{2} \rho \sigma \eta_0 \left[ \frac{e^{\Delta\alpha L} - 1}{\Delta\alpha} \right] \quad (1)$$

Where, on the right hand side, we have added a factor of  $\frac{1}{2}$  to account for the backward propagating signal that is not collected in the current configuration of our experimental setup.  $\Delta\alpha = \alpha(\omega_p) - \alpha(\omega_s)$  is the difference between the waveguide losses  $\alpha(\omega_p)$  and  $\alpha(\omega_s)$  for pump and Stokes frequencies respectively. The term in brackets converges to  $L$  when  $\Delta\alpha \rightarrow 0$ , as can

be seen by expanding the exponent. The contribution due to the quantity  $\Delta\alpha$  is generally small for small Stokes shifts and shorter waveguide lengths.

The measurement setup is similar to that reported in [3]. A tunable Ti-Sapphire CW laser emitting at 785 nm is coupled to the waveguide by end-fire coupling using an aspheric lens of effective focal length 8 mm (NA = 0.5). The incident polarization is set to the TE or TM mode of the waveguide using a half-wave-plate. The Raman signal (Stokes) collected in the waveguide and co-propagating with the pump is then collimated out of the chip via an achromatic objective (50x, NA = 0.9). The Raman signal is filtered from the strong pump using an edge filter blocking light below 790 nm. The Raman spectrum is then focused to a single-mode optical fiber (cutoff = 770 nm) using a parabolic mirror of 15 mm effective focal length (NA = 0.2) and measured using a commercial spectrometer (AvaSpec-ULS2048XL). Because of the edge filter, the pump transmission is optimized and measured at 800 nm wavelength at the position of the spectrometer. The pump transmission at 800 nm is verified to be practically the same as for the pump wavelength 785 nm without the filter. An additional polarizer at the signal collection side is used so as to only collect light of a given polarization mode.

The input laser power is set at 40 mW, with an estimated  $8 \pm 1$  dB coupling loss per chip-facet.  $\text{Si}_3\text{N}_4$  strip waveguides of widths  $w = 550$  nm and  $w = 700$  nm, as well as  $\text{Si}_3\text{N}_4$  slot waveguides with slot width  $s = 150$  nm and total waveguide width  $w = 700$  and  $w = 800$  are studied experimentally. The waveguides are wound as spirals (typical footprint:  $800 \mu\text{m} \times 500 \mu\text{m}$ ) with bend radius  $50 \mu\text{m}$  and  $150 \mu\text{m}$  for strip waveguides and slot waveguides respectively, so that the bend losses are negligible.

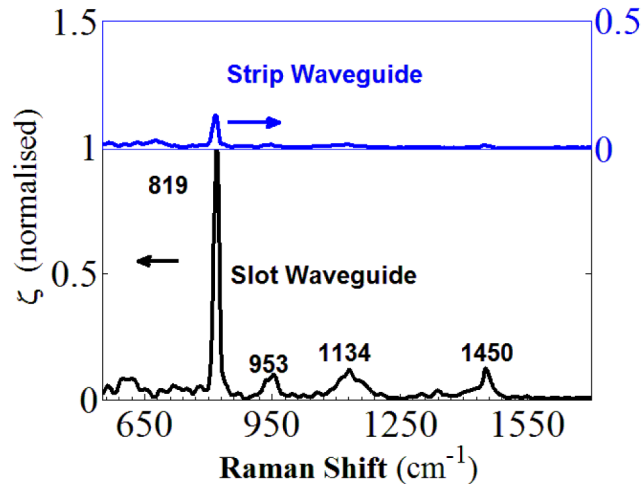


Fig. 2. Typical evanescently measured Raman spectra (normalized to 819/cm peak from slot waveguide) of IPA after background subtraction. The case shown is for excitation and collection by a TE-mode, pump power of 40 mW,  $8 \pm 1$  dB coupling losses per facet and integration time of 5 s. The black spectrum is obtained using a  $w = 700$  nm slot waveguide with  $s = 150$  nm. The blue spectrum is obtained by using 700 nm wide  $\text{Si}_3\text{N}_4$  strip waveguides and is shifted vertically for clarity (with blue axes). We observe an enhancement of the signal by more than a factor six as expected theoretically for TE modes.

$\text{Si}_3\text{N}_4$  waveguide circuits used for the experiments were fabricated on 200 mm silicon wafer containing a stack of  $2.2 \mu\text{m} - 2.4 \mu\text{m}$  thick high-density plasma chemical vapor deposition (HDP-CVD) silicon oxide ( $\text{SiO}_2$ ) and 220 nm thick plasma-enhanced-CVD (PECVD)  $\text{Si}_3\text{N}_4$  [12]. The structures were patterned with 193 nm optical lithography and subsequently etched by the fluorine based inductive coupled plasma-reactive ion-etch process to get the final structure.

Pure Isopropyl Alcohol (IPA) with a density  $\rho = 7.87 \times 10^{21}$  molecules/cm<sup>3</sup> is used as an analyte to compare the Raman signal strength for several waveguide geometries. IPA droplets are drop-casted with a pipette on top of the waveguides and cover the entire waveguide region of interest as seen with a camera from top. The Raman spectra are extracted by fitting the background spectrum with truncated polynomials as explained in [3, 17] and then subtracting it. Figure 2 shows a typical Raman spectrum of IPA obtained using such a procedure for  $w = 700$  nm strip waveguide and  $w = 700$  nm slotted waveguides with  $s = 150$  nm. As a main highlight, we observe enhanced signal for slotted waveguides, while we can clearly distinguish all the major peaks of IPA in both spectra. The IPA peak corresponding to the C-C-O vibration at  $819 \text{ cm}^{-1}$  wavenumber (839 nm, for 785 nm pump) is used as reference to compare the values of  $\eta_0$  for several waveguides. The  $\eta_0$  is estimated by first converting the total analog to digital converter (ADC) counts to the corresponding power in units of Watts. This is done by dividing the ADC counts with the corresponding integration time (typically 1-5 seconds) and the measured sensitivity ( $19 \times 10^6$  counts/ms/ $\mu\text{W}$ ) of the spectrometer near the wavelength corresponding to the IPA peak. We take  $\sigma = 7.9 \times 10^{-31} \text{ cm}^2/\text{sr}/\text{molecule}$  for the  $819 \text{ cm}^{-1}$  line which is calculated by using the value measured at 488 nm in [18] and applying the  $1/\lambda_0^4$  dependence of the scattering cross-section [4].

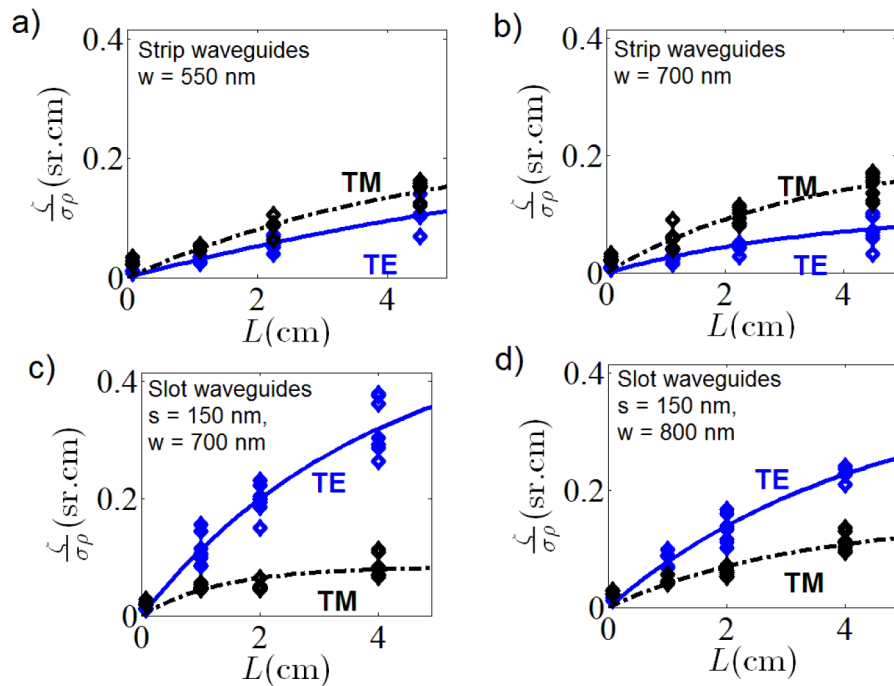


Fig. 3. Experimental data from the Raman peak of IPA at  $819 \text{ cm}^{-1}$  a) strip waveguides,  $w = 550$  nm, b) strip waveguides,  $w = 700$  nm, c) slot waveguides,  $w = 700$  nm,  $s = 150$  nm d) slot waveguides,  $w = 800$  nm,  $s = 150$  nm. Diamonds: experimental values. Lines: LSE fit of  $\zeta(L)$  as per Eq. (1). Black diamond and black dashed lines: TM polarized excitation and collection. Blue diamond and blue solid lines: TE polarized excitation and collection.

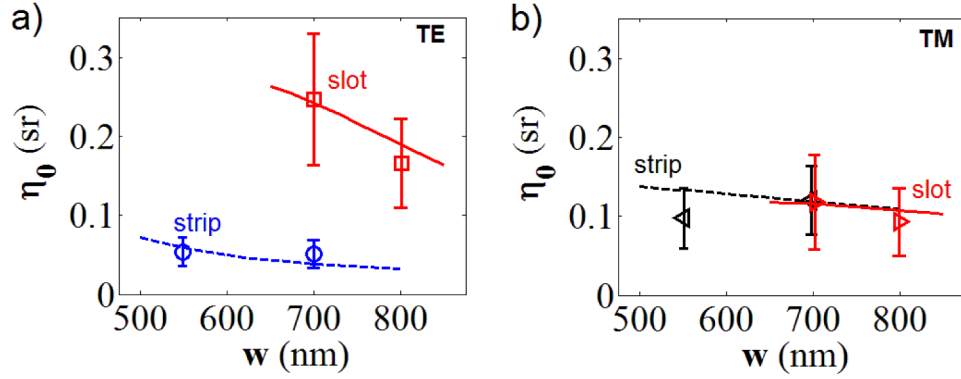


Fig. 4. The theoretical and experimental values of  $\eta_0$  obtained for a) TE modes and b) TM modes of  $\text{Si}_3\text{N}_4$  waveguides. The markers represent the estimated experimental values obtained from the LSE fit of the experimental data of Fig. 3 with Eq. (1). The error bars represent the measurement and estimation errors. Lines represent the theoretical curves obtained from Eq. (A.11). The red solid lines are the theoretical curve for slot waveguides with  $s = 150$  nm. The blue and black dashed lines are the theoretical curves for TE and TM polarizations respectively for strip waveguides. Circle: TE polarization, strip waveguides. Left handed triangles: TM polarization, strip waveguides. Right handed triangles: TM polarization, slot waveguides. Square: TE polarization, slot waveguides.

Four chips containing different waveguide dimensions and geometries were diced from different locations on a wafer and measured three times for the experiments. Figure 3 shows the experimental data for the guided power efficiency  $\zeta(L)$  normalized with  $\rho\sigma$ , the product of density and the cross section of IPA. The normalization with  $\rho\sigma$  renders the curve directly related to  $\eta_0$ . A considerable spread in the experimental values of  $\zeta(L)$  can be observed for a given waveguide length. This spread comes mainly from variation of the waveguide properties among the several waveguides on several chips and from the variation of the transmitted power caused by mechanical instability of the stages used for coupling, shot-noise of the laser and laser power drifts. The variation is particularly high for slotted waveguides due to variability of the slot width during the etching process. Variations in the thickness of  $\text{SiO}_2$  and  $\text{Si}_3\text{N}_4$  across the wafer during deposition also leads to a spread in the observed  $\zeta(L)$ . Another important source of variation is side-wall roughness of the waveguides due to imperfect waveguide etching which has not been taken into account in our theory, but which may affect the coupling of the Raman signal to the waveguide.

We implemented a Least Square Error (LSE) fitting algorithm to compare the measured data with the theoretical model. The average guided power efficiencies  $\zeta(L)$  can be fitted with the model described by Eq. (1) with mean  $R^2$  value of 0.96 indicating a good fit [19]. The LSE fit yields estimated values of  $\eta_0$  very close to the theoretically predicted values. In Fig. 4, the estimated values of  $\eta_0$  obtained for various waveguide geometries and polarizations are compared with the theoretically determined values using Eq. (13) in the Appendix. The theoretical curves of  $\eta_0$  as a function of waveguide width  $w$  are within the error margin of the experimental data for both polarizations and the waveguide types studied. Assuming statistically independent measurement errors, the total experimental error  $\Delta_{\text{tot}}$  is estimated by:

$$\Delta_{\text{tot}} = \sqrt{\Delta(P_{\text{tx}})^2 + \Delta(\sigma)^2 + \Delta(P_{\text{col}})^2 + (1 - R^2)} \quad (2)$$

where,  $\Delta(\sigma)$  ( $= \pm 10\%$ ) is the error in the cross-section value [18],  $\Delta(P_{\text{tx}})$  ( $= \pm 20\%$ ) is the error in the measurement of transmitted power,  $\Delta(P_{\text{col}})$  ( $= \pm 25\%$ ) is the error in the measurement of the sensitivity of the spectrometer. The last term in Eq. (2) approximates the error due to the fit [19].

For 700 nm wide  $\text{Si}_3\text{N}_4$  strip waveguides, the average efficiency  $\eta_0$  for TM polarization is approximately 2.5 times larger than for TE excitation. For 700 nm wide  $\text{Si}_3\text{N}_4$  slot waveguides ( $s = 150$  nm) excited with TE polarized light, about 6 fold enhancement of the estimated  $\eta_0$  compared to strip waveguides of the same width. Note that the wider waveguides lead to reduced  $\eta_0$ . In the next section, we will investigate and explain these results using the model just validated.

### 3. Analysis of $\eta_0$ for $\text{Si}_3\text{N}_4$ , $\text{TiO}_2$ and SOI channel waveguides

Having established the relevance of our model, we elaborate the experimental results obtained in the previous section with the theory and extend the theoretical analysis to  $\text{TiO}_2$  and SOI waveguides. To be in line with the experimental parameters used for the experiments with the  $\text{Si}_3\text{N}_4$  waveguides, we perform simulations with an excitation wavelength  $\lambda_0 = 785$  nm. The refractive indices of the core,  $\text{SiO}_2$  undercladding and IPA upper cladding are respectively taken to be  $n_{\text{sin}} = 1.89$ ,  $n_{\text{ox}} = 1.45$  and  $n_{\text{ipa}} = 1.37$ . In case of SOI waveguides,  $\lambda_0 = 1550$  nm was chosen because of a low optical absorption. The refractive index of silicon is taken to be  $n_{\text{si}} = 3.44$ . As for  $\text{TiO}_2$  waveguides, the refractive index  $n_{\text{TiO}_2} = 2.4$  reported in [15] is used. For the  $\text{TiO}_2$  case we study  $\eta_0$  at  $\lambda_0 = 785$  nm and also at  $\lambda_0 = 1064$  nm. The latter choice of  $\lambda_0$  corresponds to a material wavelength comparable to that of SOI (at  $\lambda_0 = 1550$  nm) and  $\text{Si}_3\text{N}_4$  (at  $\lambda_0 = 785$  nm). The aforementioned choice of the comparable material wavelengths ensures similar fabrication constraints and practical waveguide dimensions for single mode operation. The height of the waveguides is fixed at  $h = 220$  nm for all waveguide types, which is a typical deposition thickness during the fabrication of  $\text{Si}_3\text{N}_4$  and  $\text{TiO}_2$  waveguides, and also a typical silicon thickness for SOI waveguides. The conversion efficiency  $\eta_0$  was calculated using Eq. (13) with COMSOL finite elements mode solver.

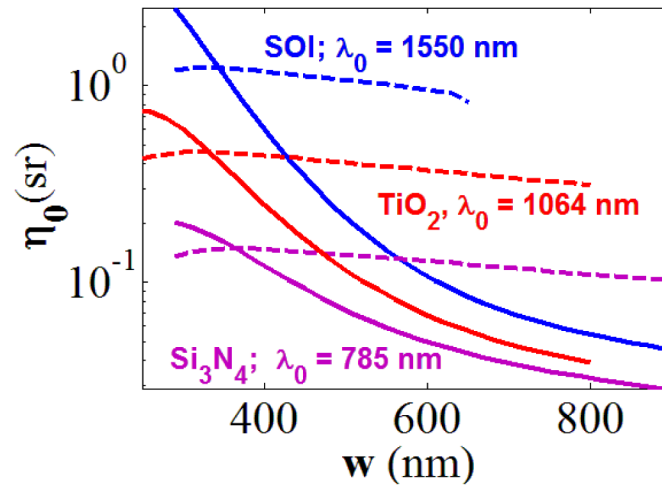


Fig. 5. Theoretical conversion efficiency curves for strip waveguides as a function of total waveguide width  $w$  for different material systems and the corresponding excitation wavelengths. Blue, red and magenta colors are respectively for SOI,  $\text{TiO}_2$  and  $\text{Si}_3\text{N}_4$  cores. Solid lines: TE polarized excitation and collection. Dashed lines: TM polarized excitation and collection. Only the curve segments corresponding to single mode operation from the cut-off width are shown. Note that y-axis in log scale.

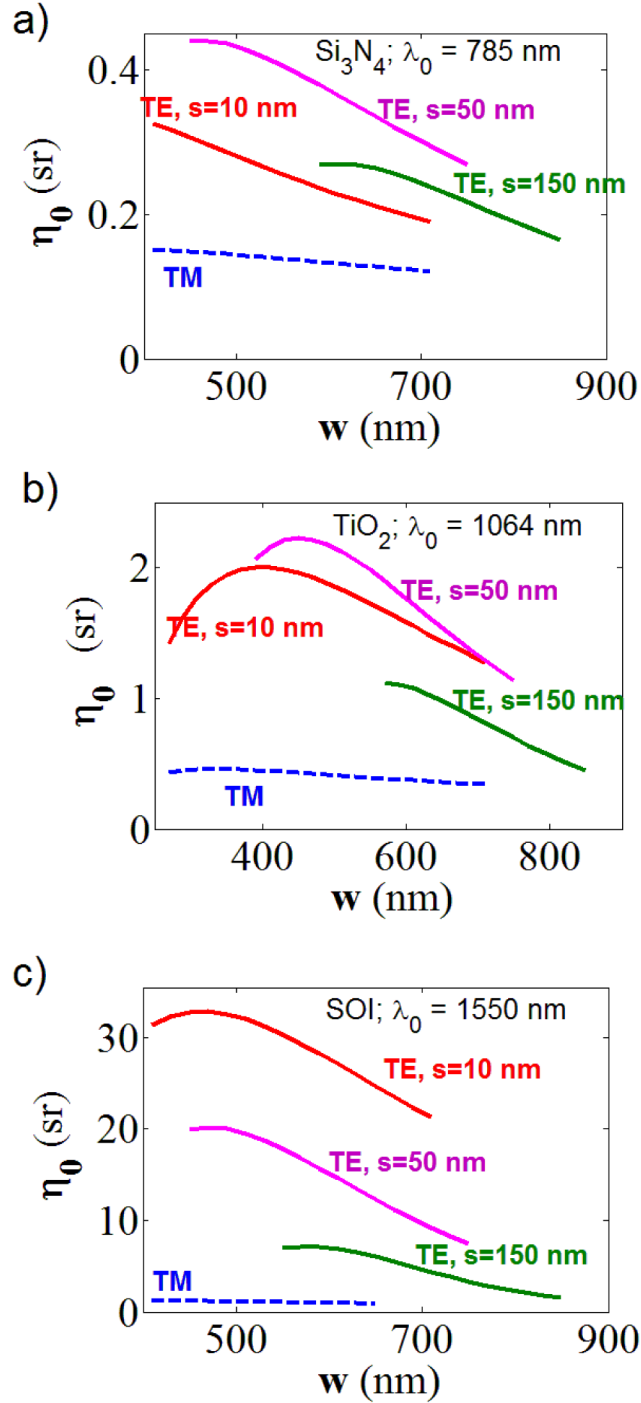


Fig. 6. Theoretical conversion efficiency curves for slot waveguides for a)  $\text{Si}_3\text{N}_4$  core with  $\lambda_0 = 785$  nm, b)  $\text{TiO}_2$  core with  $\lambda_0 = 1064$  nm c) silicon core with  $\lambda_0 = 1550$  nm. The solid lines: TE polarized excitation and collection. Dashed lines: TM polarized excitation and collection. Green, magenta and red lines are respectively for slot width of 150 nm, 50 nm and 10 nm. Only the curve segments corresponding to single mode operation from the cut-off width are shown.

In Fig. 5 we show theoretical conversion efficiency  $\eta_0$  for randomly distributed particles lying uniformly in the upper cladding of Si<sub>3</sub>N<sub>4</sub>, TiO<sub>2</sub> and SOI strip waveguides of several waveguide widths  $w$  corresponding to the single mode operation of the waveguides. As the waveguide width is increased, initially  $\eta_0$  increases to a maximum corresponding to an optimal mode confinement in the core and the cladding. Once this condition is reached, further increase in the width leads to a decrease in  $\eta_0$  owing to more confinement of the modal field in the core. We observe this irrespective of the waveguide type, polarization or core material. This is because the increase in the waveguide width increases the confinement of the mode in the core thereby reducing the interacting field in the upper cladding region of the analytes. For strip waveguides, TM polarization generally performs better than TE polarized modes and its sensitivity to the waveguide width is smaller. The discontinuity of the electric field at the core - top cladding interface of the TM modes leads to higher field at the analyte location. The increased field and larger interaction volume present on the top cladding for TM modes (owing to high width-height aspect ratio) results in higher  $\eta_0$ . Since the electric field in the TM mode is discontinuous in the perpendicular direction, only substantial changes in waveguide height  $h$  vary the TM field significantly. For a typical 600 nm wide strip waveguide, TM excitation in comparison to the TE excitation, leads to more than 2.5, 4 and 5 times more efficiency respectively for Si<sub>3</sub>N<sub>4</sub> (at  $\lambda_0 = 785$  nm), TiO<sub>2</sub> ( $\lambda_0 = 1064$  nm), and Si ( $\lambda_0 = 1550$  nm) waveguides.

In Fig. 6,  $\eta_0$  for slotted waveguides with various slot widths  $s = 10$  nm, 50 nm, and 150 nm, and waveguide widths  $w$  (inclusive of the slot) is shown for Si<sub>3</sub>N<sub>4</sub>, TiO<sub>2</sub> and SOI waveguides. In case of TE polarized modes, slotted waveguides generally perform much better than strip waveguides and the value of  $\eta_0$  increases as  $s$  decreases. This can be attributed to the enhancement of the TE-field in the slot region as  $s$  is decreased. However, there is an optimum  $s$  whence  $\eta_0$  starts to decrease. This originates from a reduction in the interaction volume within the slot region as  $s$  is decreased. The optimum  $s$  is near 50 nm, 30 nm and 10 nm for respectively Si<sub>3</sub>N<sub>4</sub> (operating at  $\lambda_0 = 785$  nm), TiO<sub>2</sub> waveguides ( $\lambda_0 = 1064$  nm) and SOI waveguides ( $\lambda_0 = 1550$  nm). As expected, due to the continuity of the electric field, the field enhancement in the slot is much less in case of TM polarization (Fig. 7); hence, the effect of  $s$  is not significant in case of TM polarization.

In Fig. 8 we compare the conversion efficiency  $\eta_0$  of TiO<sub>2</sub> waveguides for  $\lambda_0 = 785$  nm and  $\lambda_0 = 1064$  nm.  $\eta_0$  is generally higher for  $\lambda_0 = 1064$  nm because the field is confined more to the cladding where analyte is located. Due to a shorter material wavelength, the modal field is more confined to the high index TiO<sub>2</sub> region when excited at 785 nm, compared to excitation at 1064 nm. Consequently, the optimal slot width for TiO<sub>2</sub> ( $\lambda_0 = 785$  nm) is narrower: about 10 nm compared to about 30 nm  $\lambda_0 = 1064$  nm. For  $\lambda_0 = 785$  nm  $\eta_0$  also increases weakly for wider slots (such as  $150 \text{ nm} > s > 100 \text{ nm}$ ). This can be understood with the help of Fig. 7.

In Fig. 9, we show the conversion efficiency  $\eta_0$  of slot waveguides with  $s = 100$  nm, as a function of the total waveguide width  $w$  for different material systems. We observe a strong enhancement in  $\eta_0$  with the increase in the index contrast of the waveguide. Higher index contrast leads to a lower mode area, higher modal field intensity and higher field discontinuity, thus giving rise to a stronger evanescent field for interaction. From the simulation data presented in Figs. 5 and 9, we can conclude that a slot of width  $s = 100$  nm leads to about 90, 20 and 7 fold higher efficiency respectively for SOI (excited at  $\lambda_0 = 1550$  nm), TiO<sub>2</sub> ( $\lambda_0 = 1064$  nm), Si<sub>3</sub>N<sub>4</sub> ( $\lambda_0 = 785$  nm) slot waveguides of  $w = 600$  nm compared to the strip waveguide of the same dimension.

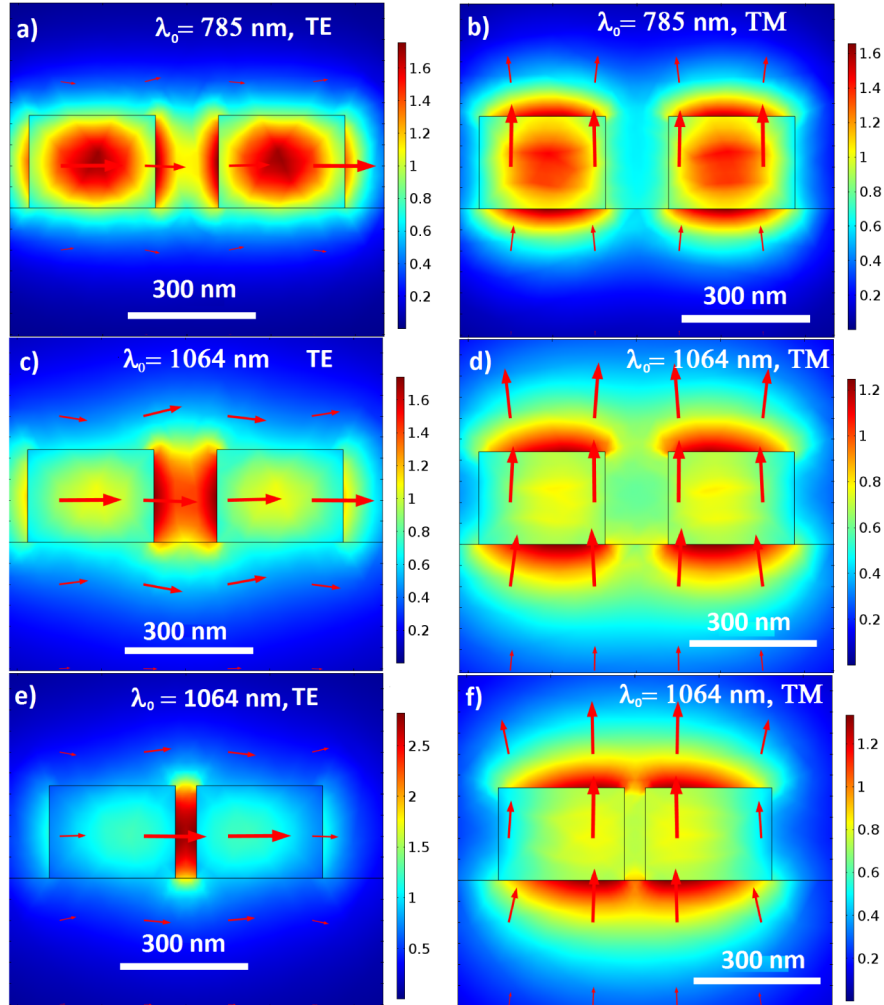


Fig. 7. Plot of the modal field of the TiO<sub>2</sub> slot waveguides for a) TE polarization for  $s = 150$  nm,  $w = 750$  nm,  $\lambda_0 = 785$  nm, b) TM polarization for  $s = 150$  nm,  $w = 750$  nm,  $\lambda_0 = 785$  nm, c) TE polarization,  $s = 150$  nm,  $w = 750$  nm,  $\lambda_0 = 1064$  nm d) TM polarization for  $s = 150$  nm,  $w = 750$  nm,  $\lambda_0 = 1064$  nm, e) TE polarization for  $s = 50$  nm,  $w = 650$  nm,  $\lambda_0 = 1064$  nm f) TM polarization for  $s = 50$  nm,  $w = 650$  nm,  $\lambda_0 = 1064$  nm. The arrow shows the electric field vector at a given location.

When comparing different waveguide systems operating at different excitation wavelengths, however, the corresponding change in the scattering cross-section also has to be taken into account. As the scattering cross-section varies approximately as  $1/\lambda_0^4$  [4], the total collected power also varies in a similar manner. We can include this correction factor and compare the respective net efficiencies for slot waveguides ( $w = 600$  nm and  $s = 100$  nm), Si<sub>3</sub>N<sub>4</sub> waveguides ( $\lambda_0 = 785$  nm), TiO<sub>2</sub> waveguides ( $\lambda_0 = 1064$  nm) and the SOI waveguides ( $\lambda_0 = 1550$  nm). After the  $1/\lambda_0^4$  correction at these respective operating wavelengths, SOI is about twice as efficient, and TiO<sub>2</sub> is about 30% more efficient than Si<sub>3</sub>N<sub>4</sub> waveguides owing to their higher index contrast.

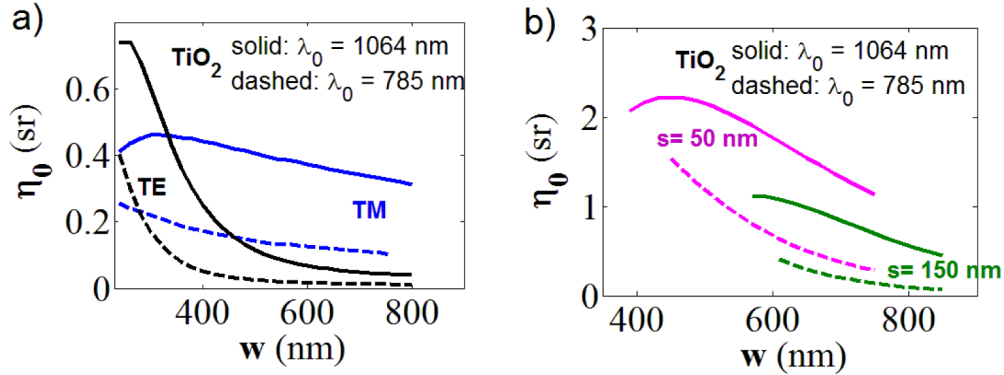


Fig. 8. Theoretical conversion efficiency curves for TiO<sub>2</sub> a) strip b) slot waveguides with  $\lambda_0 = 785$  nm (dashed lines) and  $\lambda_0 = 1064$  nm (solid lines). Black and blue curves: strip waveguides. Green: slot waveguides,  $s = 150$  nm. Magenta: slot waveguide,  $s = 50$  nm. The values of  $\eta_0$  for TM polarization for all the slot widths (data not shown) do not differ significantly from the values for strip waveguides. Only the curve segments corresponding to single mode operation from the cut-off width are shown.

Note that in Figs. 6 and 9,  $\eta_0 > 4\pi$  sr, for SOI waveguides in a certain range of waveguide dimensions. This is a result of high importance. To appreciate this, we apply Eq. (12) for free space beams with  $\eta_0 = 4\pi$  and integrate  $dz$  arbitrarily. This is possible in an ideal situation when we can collect the scattered light perfectly from total solid angle of  $4\pi$  sr, and if particles are excited with a diffraction-less beam so that  $dz$  in Eq. (12) can be integrated arbitrarily. Thus, we conclude that due to enhanced excitation and emission (Purcell enhancement) near the high index contrast waveguides, the overall efficiency of excitation and collection of a practical single mode waveguide can be higher than the ideal free space excitation and collection. For a realistic diffraction-limited free-space microscope system, however, the collection and excitation depth of focus are limited due an inverse relationship between the collection angle and the depth of focus. Hence, waveguide systems, in general, perform much better than realistic free space optical systems [5].

Although the current experiments and simulations are performed for IPA as the analyte in the upper cladding, the experimental and theoretical assessments have also been performed using other analytes such as acetone, dimethyl sulfoxide, their aqueous solutions and also clinically relevant solutions, such as glucose solution. If the upper cladding refractive index varies, the confinement properties of the waveguide mode also changes. Consequently, the conversion efficiency will vary via Eq. (9) in the Appendix. Nevertheless, the qualitative conclusions discussed in this article are applicable for analytes with refractive index in the range 1.3-1.44. For analytes with refractive indices significantly different from IPA ( $n = 1.37$ ),  $\eta_0$  can be calculated using Eq. (9) and Eq. (13).

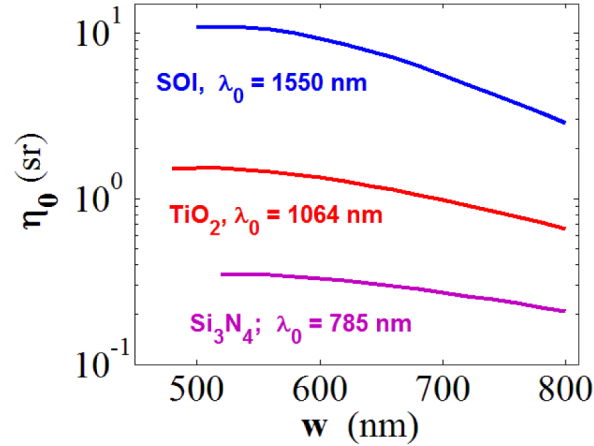


Fig. 9. The conversion efficiency  $\eta_0$  of slot waveguides with  $s = 100$  nm as a function of total waveguide width  $w$  for different material systems and corresponding excitation wavelengths. Note that y-axis in log scale.

#### 4. Conclusion

Based on our measurements of evanescently collected Raman signals with  $\text{Si}_3\text{N}_4$  slot and strip waveguides, we have been able to validate a theoretical model for the collection efficiency of generic channel waveguides. Using the model, we have investigated the effect of waveguide geometry, core refractive index and polarization on the overall efficiency of evanescent excitation and collection of spontaneous Raman scattering. Due to enhanced excitation and emission near the high index contrast waveguides, the overall efficiency of excitation and collection of a practical single mode waveguide can be higher than the ideal free space excitation and collection. We have shown that when excited with TE polarized modes, slot waveguides have the highest efficiency. Specifically, we have shown that a slot of width  $s = 100$  nm leads to approximately 90, 22 and 7 fold more efficiency respectively for SOI (excited at  $\lambda_0 = 1550$  nm),  $\text{TiO}_2$  ( $\lambda_0 = 1064$  nm),  $\text{Si}_3\text{N}_4$  ( $\lambda_0 = 785$  nm) for slot waveguides compared to the strip waveguides of the similar dimensions. In case of strip waveguides of typical dimensions, excitation and collection of Raman signal using TM polarized modes leads to higher collection efficiency than for TE polarization. Specifically, for 600 nm wide strip waveguides, TM excitation leads to more than 2.5, 4 and 5 times more efficiency for  $\text{Si}_3\text{N}_4$ ,  $\text{TiO}_2$  and Si core compared to TE excitation. The investigated slot and strip waveguides for this result can be fabricated with current Deep-UV lithography technology. The results of this paper can also be used for integrated light sources based on evanescent interaction of the waveguide modes with quantum dots [20], rare-earth dopants [21] or III-V epitaxial layers [22]. Finally, we conclude that owing to their higher index contrast, SOI waveguides excited with 1550 nm and emerging  $\text{TiO}_2$  waveguide platform operating at 1064 nm are good candidates for evanescent Raman or fluorescence sensing and light generation.

#### Appendix: Theoretical model of scattering near waveguides

An electromagnetic field  $\mathbf{E}$  induces a dipole moment  $\mathbf{d}_0 = \alpha \mathbf{E}$  for a particle with scalar polarizability  $\alpha$ . In the context of off-resonance, non-degenerate and adiabatic vibrational transitions corresponding to a pump frequency  $\omega_p$  and a Stokes frequency  $\omega_s$ ,  $\mathbf{d}_0 = \alpha(\omega_p, \omega_s) \mathbf{E}$  and  $\alpha(\omega_p, \omega_s)$  is called Placzek polarizability [4].  $\alpha(\omega_p, \omega_s)$  can be expressed in terms of the more familiar scattering cross-section  $\sigma$  using  $\lambda_0^4 \sigma = k_v \alpha^2$ , where  $2\pi c/\lambda_0 \approx \omega_p \approx \omega_s$  and  $k_v = 1.26 \times 10^{23} \text{ C}^{-2}\text{V}^2\text{m}^2$  is a universal constant related to the fine structure constant characterizing the coupling between electronic charge and the electromagnetic field [4]. Then we can write:

$$|\vec{d}_0(\vec{r}_0, \omega_s)|^2 = \frac{\lambda_0^4}{k_v} \sigma(\omega_p, \omega_s) |\vec{E}(\vec{r}_0, \omega_p)|^2 \quad (3)$$

We assume that the particle is located at the position  $\mathbf{r}_0$  in the neighborhood of a channel photonic waveguide defined by a dielectric function  $\varepsilon(\mathbf{r})$  (Fig. 1). Consider its interaction with a guided mode traveling with group velocity  $v_g$  and carrying a power  $P_{pump}$ . For simplicity, we also assume that the waveguide core has a sufficiently small cross-section area so that only fundamental guided modes exist. If the power-normalized modal field distribution is  $\mathbf{e}_m(\mathbf{r})$ , then the electric field component due to the mode is given by [23]:

$$|\vec{E}(\vec{r}_0, \omega_p)|^2 = \frac{P_{pump} |\vec{e}_m(\vec{r}_0, \omega_p)|^2}{v_g(\omega_p) \iint_{\infty} \varepsilon_0 \varepsilon(\vec{r}, \omega_p) |\vec{e}_m(\vec{r}, \omega_p)|^2 d\vec{r}} = \frac{P_{pump}}{\varepsilon_0 v_g(\omega_p) \tilde{A}_{eff}(\vec{r}_0, \omega_p)} \quad (4)$$

Where, analogous to [12], we use the following as a definition of effective mode area:

$$\tilde{A}_{eff}(\vec{r}_0, \omega_p) \equiv \frac{\iint_{\infty} \varepsilon(\vec{r}, \omega_p) |\vec{e}_m(\vec{r}, \omega_p)|^2 d\vec{r}}{|\vec{e}_m(\vec{r}_0, \omega_p)|^2} \quad (5)$$

A molecule with dipole strength  $\mathbf{d}_0$  oscillating at frequency  $\omega_s$ , as given by Eq. (3), would radiate power  $P_0$  in free space given by,

$$P_0 = \frac{\omega^4 |\vec{d}_0|^2}{12\pi\varepsilon_0 c^3} = \frac{4\pi^3}{3k_v \varepsilon_0^2} \frac{\sigma(\omega_p, \omega_s) n_g(\omega_p)}{\tilde{A}_{eff}(\vec{r}_0, \omega_p)} P_{pump} \quad (6)$$

However, due to the presence of the waveguide, the radiation rate is modified and the power that is coupled to the waveguide mode in both directions can be related to the power of free space emission as [12]:

$$P_{wg}(\vec{r}_0, \omega_s) = P_0 \frac{3}{4\pi} \frac{n_g(\omega_s)}{n(\omega_s)} \frac{\lambda_s^2}{\tilde{A}_{eff}(\vec{r}_0, \omega_s)} \quad (7)$$

Equation (7) assumes there is only a radiative decay pathway and the power is low enough so that we are in a weak coupling regime and any saturation effects can be neglected. These are reasonable assumptions for scattering problems encountered in photonics. Combining, Eq. (6) and Eq. (7), we arrive at the equation for waveguide scattering efficiency due to an arbitrary particle:

$$\frac{P_{wg}(\vec{r}_0, \omega_s)}{P_{pump}} = \frac{\pi^2}{\varepsilon_0^2 k_v} \frac{n_g(\omega_p) n_g(\omega_s)}{n(\omega_s)} \frac{\lambda_s^2 \sigma(\omega_p, \omega_s)}{\tilde{A}_{eff}(\vec{r}_0, \omega_p) \tilde{A}_{eff}(\vec{r}_0, \omega_s)} = \Lambda_{wg}(\vec{r}_0, \omega_p, \omega_s) \sigma(\omega_p, \omega_s) \quad (8)$$

Referring to the terminology in particle scattering theory [24], we denominate  $\Lambda_{wg}$  as the *integrated-luminosity* of the waveguide.  $\Lambda_{wg}$  gives a measure of the fraction of power scattered back to the waveguide for a given particle in its surrounding taking the waveguide enhancement effects into account.  $\Lambda_{wg}$  is a function of the position of the particle and the electromagnetic mode as defined by the waveguide dielectric function and has *sr. m<sup>-2</sup>* as its SI unit. Note that we have not assumed any specific geometry, dielectric function, polarization and specifics of the modes to arrive at Eq. (8). Hence, Eq. (8) is generally applicable to any set of orthonormal modes. Further, the analysis can be modeled in a similar manner in case of fluorescence or other resonant transition problems, by taking into account the corresponding transition polarizability and cross section.

If the pump and stokes frequencies are sufficiently near, i.e.  $\omega_p \approx \omega_s \approx \omega = 2\pi c/\lambda_0$ , such that the corresponding group indices and the effective areas are comparable,

$$\Lambda_{\text{wg}}(\vec{r}_0, \omega_p \approx \omega_s \approx \omega) = \frac{1}{n(\omega)k_v} \left( \frac{\pi}{\epsilon_0} \frac{n_g(\omega)\lambda_0}{\tilde{A}_{\text{eff}}(\vec{r}_0, \omega_p)} \right)^2 \quad (9)$$

Equation (9) with assumption  $\omega_p \approx \omega_s \approx \omega = 2\pi c/\lambda_0$ , is a reasonable estimate of the  $\Lambda_{\text{wg}}$  parameter for small Raman shifts and the waveguide geometries discussed in this paper. The difference is <10% for stokes shifts up to 1600/cm for a pump of 785 nm, as verified by more rigorous simulations carried out using Eq. (8) in COMSOL finite elements mode solver and Lumerical mode solver.

For a random ensemble of particles emitting incoherently lying close to an arbitrarily shaped waveguide with a uniform volume density  $\rho$ , the total scattering efficiency by all the particles is given by:

$$\frac{P_{\text{wg}}(\vec{r}_0, \omega_s)}{P_{\text{pump}}} \equiv \sigma(\omega_p, \omega_s) \rho \iiint_V \Lambda_{\text{wg}}(\vec{r}_0, \omega_p, \omega_s) d\vec{r} \quad (10)$$

For an infinitesimal waveguide section of length  $dz$ , one can define the *conversion efficiency*  $\eta_0$  by:

$$\eta_0(dz, \omega_p, \omega_s) \equiv \frac{d}{dz} \iiint_V \Lambda_{\text{wg}}(\vec{r}_0, \omega_p, \omega_s) d\vec{r} = \iint_S \Lambda_{\text{wg}}(\vec{r}_0, \omega_p, \omega_s) d\vec{r} \quad (11)$$

such that, the power  $dP_{\text{wg}}$  collected by the waveguide section from the particles is

$$\frac{dP_{\text{wg}}(\omega_s)}{P_{\text{pump}}} = \eta_0(dz, \omega_p, \omega_s) \rho \sigma(\omega_p, \omega_s) dz \quad (12)$$

The conversion efficiency  $\eta_0$  for a given waveguide section is an important parameter. It has  $sr$  as its unit. Like  $\Lambda_{\text{wg}}$ , it is determined uniquely by the electromagnetic mode as defined by the waveguide dielectric function. An analogy with free-space excitation  $\eta_0$  can be understood to be related to the excitation and collection solid-angle. If the nanophotonic waveguide is translationally invariant across its length and the scattering particles lie uniformly in the upper cladding, then for any arbitrary length segment, the conversion efficiency  $\eta_0$  is invariantly given by:

$$\eta_0(\omega_p, \omega_s) = \iint_{\text{up.clad}} \Lambda_{\text{wg}}(\vec{r}_0, \omega_p, \omega_s) d\vec{r} \quad (13)$$

Here, the integral is carried out in the upper cladding region where the scattering particles are located.

### Acknowledgment

The authors acknowledge the ERC advanced grant InSpectra for partial funding as well as imec, Leuven for fabrication of the waveguides.